Proceedings of the 7th International Conference on Mechanics and Materials in Design
Albufeira/Portugal 11-15 June 2017. Editors J.F. Silva Gomes and S.A. Meguid.
Publ. INEGI/FEUP (2017)

PAPER REF: 6615

CORROSION FATIGUE BEHAVIOR OF STEELS IN BIOFUELS

Sven Käfer[1(*)], Tobias Melz[1,2], Heinz Kaufmann[2], Christopher Tom Engler[3], Georg Anderson[3], Matthias Oechsner[3]

[1]Research Group for System Reliability, Adaptive Structures, and Machine Acoustics SAM, Technische Universität Darmstadt, Darmstadt, Germany
[2]Fraunhofer Institute for Structural Durability and System Reliability LBF, Darmstadt, Germany
[3]State Material Testing Institute and Institute for Materials Technology, Technische Universität Darmstadt Darmstadt, Germany
[(*)]*Email:* sven.kaefer@sam.tu-darmstadt.de

ABSTRACT

In this contribution, the impact of corrosion fatigue was investigated on notched and unnotched specimens of chromium stainless steel 1.4016 (X6Cr17), in air and E85 biofuel (gasoline fuel with 85% ethanol added), and of quenched and tempered steel 1.7228 (50CrMo4), in air and B20 biodiesel (biodiesel with 20% soy methyl ester added). The results were obtained at a stress ratio of R = 0 using different testing rigs to investigate the influence of test frequencies (f = 20, 150, 300/500 Hz).

Keywords: ***c***orrosion fatigue, biofuel, 1.4016, 1.7228

INTRODUCTION

Engine components, such as injection systems, encounter a large number of load cycles ($N>10^7$) during their lifetime and are exposed to potentially corrosive media such as blended fuels. Currently, the automotive companies reach their durability specifications for engine components by using stainless steels with lower strength but high corrosion resistance, specifically oversizing components, because there is not yet much known about the very high cycle corrosion fatigue behaviour of high-strength steels in biofuels. Indeed, investigations show that biofuels significantly reduce the number of load cycles to failure of engine components (Schmidt, 2013). Due to the higher amount of biogenic components, the hygroscopic properties of biofuels have increased, causing an input of different kinds of corrosive substances, e.g. chlorides that are dissolved in water. Therefore, it is essential to investigate the corrosive impact of fuels with biogenic components by performing corrosion fatigue tests.

To examine the corrosive impact and to obtain results that can be transferred to real engine components, four different geometries (unnotched, notched) were investigated. All samples were machined from round semi-finished bars.

SPECIMENS, MATERIALS, MEDIA AND TESTING

Materials and specimens

The materials examined in this work were a chromium stainless steel 1.4016 (X6Cr17) and a quenched and tempered steel 1.7228 (50CrMo4). Both steels are used for engine components such as injection valves and high pressure pumps that are exposed to biogenic gasoline fuels.

These materials were received as wrought semi-finished round bars with a diameter of 19 mm (1.4016) or 28 mm (1.7228). The chemical compositions of the materials were determined by spectral analysis and are shown in Table 1. The mechanical properties are shown in Table 2.

Table 1 - Chemical composition of tested materials in weight%

Material	C	Si	Mn	P	S	Cr	Mo	Ni
1.4016	0.069	0.525	0.477	0.031	<0.010	16.450	0.061	0.211
1.7228	0.493	0.259	0.691	<0.010	0.011	1.010	0.185	0.026

Table 2 - Mechanical properties of tested materials

Material	Yield strength $R_{p0.2}$ [MPa]	Tensile strength R_m [MPa]	Young's modulus E [GPa]	Elongation at fracture A [%]	Hardness [HV 10]
1.4016	730	830	198	16	246/356
1.7228	1000	1090	208	14	364

Fig. 1 shows the microstructures in the cross-section of the delivered round bars of the investigated materials. On the left hand side, the ferritic-perlitic microstructure of the 1.4016 steel with chromium carbide segregations along the grain boundaries is shown. Despite fast cooling rates, ferritic-chromium steels tend to exhibit chromium carbides. This will result in a potential susceptibility to intergranular corrosion. On the right hand side, the martensitic microstructure of the 1.7228 steel with martensitic needles is shown. In the core material, segregation can been seen, which results in a slightly inhomogeneous matrix.

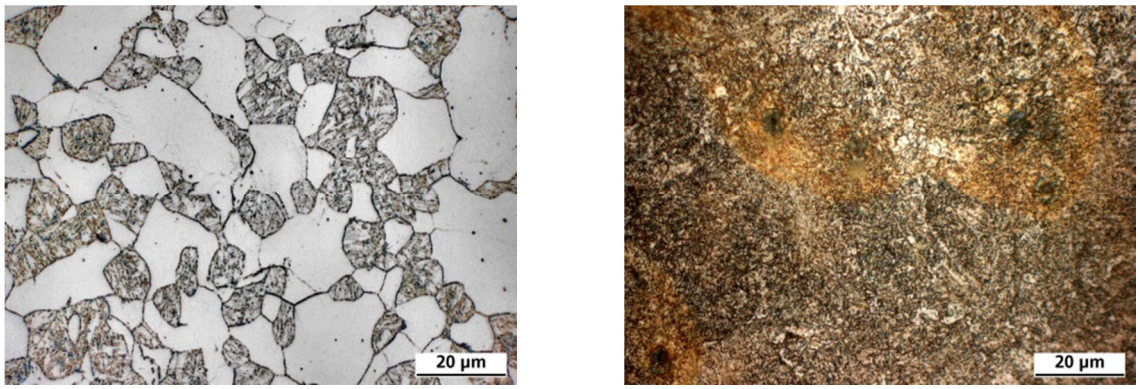

Fig. 1 - Microstructures of 1.4016 steel (left) and 1.7228 steel (right)

To examine the corrosive impact and to obtain results that can be transferred to engine components, four different geometries were investigated. All samples were turned from round semi-finished bars as mentioned above. Both of the unnotched geometry with a theoretical stress concentration factor of $K_t \approx 1$ are shown in Fig. 2. The specimens with a diameter of Ø4 mm were tested at the servo hydraulic test rig and the resonance actuator; those with a smaller diameter of Ø3 mm were tested with a piezoelectric actuator. The notched specimens have a circular notch with a radius of 1 mm for the Ø6 mm specimens and 0.6 mm for the Ø3.5 mm specimens, resulting in a stress concentration factor of $K_t \approx 2$, and these specimens are shown in Fig. 3. Due to the smaller nominal load capacity of the piezoelectric actuator, smaller specimen diameters (Ø3 and Ø3.5 mm) were chosen for these tests. Stress concentration factors were calculated by the linear-elastic finite element method and compared to analytically calculated stress concentration factors using the Neuber (Neuber, 1958) and Rainer approaches (Rainer, 1978).

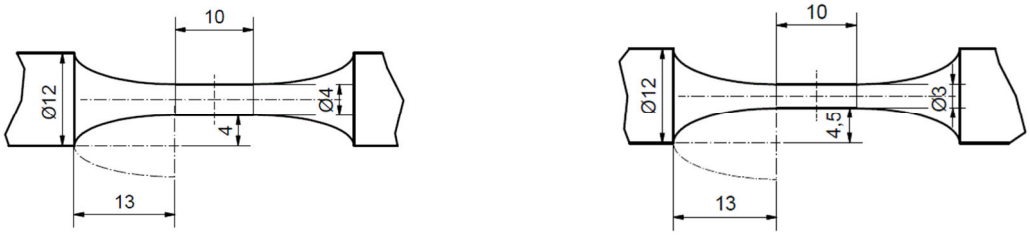

Fig. 2 - Geometries of the unnotched specimens, theoretical stress concentration factor $K_t \approx 1$

Fig. 3 - Geometries of the notched specimens, theoretical stress concentration factor $K_t \approx 2$, normalised stress gradient $\chi^* = 1.86$ mm^{-1} for Ø6 mm and $\chi^* = 3.00$ mm^{-1} for Ø3.5 mm

After the manufacturing process, the surface roughnesses and the diameters of all specimen geometries were measured randomly on 10 specimens of each type. The roughness R_z was less than 3.0 µm and the dimensions of the diameter were within the tolerance of ± 0.01 mm respectively. Due to the turning process, compressive residual stresses were induced near the surface of the specimens.

The investigated unnotched specimens revealed compressive residual stresses in the axial direction of about 400 MPa on average and the notched specimens had a compressive residual stress of about 200 - 300 MPa, which decreased with depth from the specimen surface. Residual stresses converged to 0 at about 50 µm for unnotched specimens and at about 100 µm below the surface for the notched specimens.

Media

The investigations in air and biofuel were both performed at ambient room temperature. For corrosion fatigue investigations, the specimens were installed in a fuel chamber prior to mounting in the testing actuator. Before and after every use of the fuel chamber, it was sonically cleaned in ethanol. The fuel chamber was designed in glass and PTFE[1] in order for there to be no corrosive impact from the material of the chamber, as illustrated in Fig. 4.

To ensure that tests on unnotched and notched specimens had the same specimen-surface/fuel-volume ratio, two chamber sizes were adjusted accordingly. The chamber with the specimen was completely filled with biofuel with no additional air, to provide defined corrosive conditions. During the test, the temperature of the biofuel was monitored at all times. The specifications of the chosen biofuels are given in Table 3.

[1] PTFE: Polytetrafluorethylen, is a synthetic fluorpolymer also called teflon

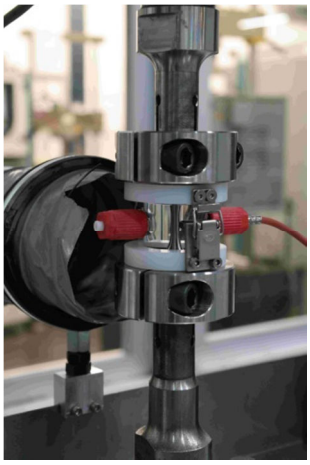

Fig. 4 - Specimen mounted in fuel chamber with temperature monitoring

Table 3 - Specifications of chosen biofuels

Biofuel	Concentrations						
	Ethanol [Vol.-%]	Soy methyl ester [Vol.-%]	Water [mg/kg]	Chloride [mg/kg]	Acetic acid [mg/kg]	Sulfuric acid [mg/kg]	Formic acid [mg/kg]
E85	85	-	9000	3	20	n/s	2
B20	-	20	200	-	-	11	-

Fatigue testing

Fatigue tests in air and biofuel were performed with three different types of test rigs in order to investigate the influence of testing frequency. Fatigue tests on the servo hydraulic test rig were carried out at a frequency f = 20 Hz up to $N = 10^7$ load cycles. Resonance actuator fatigue testing was performed at about f = 150 Hz up to $N = 10^8$ load cycles. Tests at f = 300 and 500 Hz up to $N = 5 \cdot 10^8$ load cycles were realised using a piezoelectric actuator. All investigations were carried out under axial loading in load-control with a sinusoidal-shaped load at a stress ratio of R = 0.

RESULTS

The SN-results of the investigated materials in air and in contact with potentially corrosive fuels will be shown in detail in the following.

Fatigue in air

The SN-results at 20, 150, 300 and 500 Hz load frequencies in air for the 1.4016 steel are shown in Fig. 5 and for the 1.7228 steel in Fig. 6in double logarithmic diagrams for the unnotched and notched specimens for the nominal stress amplitude $\sigma_{a,n}$. The nominal stress amplitude is plotted against the number of load cycles to failure N_f. The survival probability (10% / 50% / 90%) at a specific load level is illustrated in the diagram by three parallel SN-curves and a scatter band of T_σ. Specimens that did not fail after $N = 10^7$ load cycles on the servo hydraulic test rig, $N = 10^8$ load cycles using the resonance actuator or $N = 5 \cdot 10^8$ load cycles using the piezoelectric actuator were indicated as run-outs (arrows pointing to the right). Differently coloured symbols were used to indicate the different test rigs. All samples showed crack origins at the surface. The slope k in the medium cycle fatigue regime ($5 \cdot 10^4 <$

$N < 5 \cdot 10^5$) was evaluated by regression analysis using the test results up to the knee point N_k. The slope after the knee point N_k was estimated to be k* = 44.9 with a 5% decrease for the 1.4016 steel and to be k* = 90 with a 2.5% decrease for the 1.7228 steel of the fatigue strength per decade (Sonsino, 2007). The knee point N_k was set to $N = 5 \cdot 10^5$ load cycles for the 1.4016 steel and to $N = 1 \cdot 10^5$ load cycles for the 1.7228 steel. Referring to the normalised SN-curve proposed by (Haibach, 2006), uniform values of the parameters, knee point N_k, scatter band T_σ and slope k* after the knee point were taken as the basis for the SN-curves of the unnotched and notched specimens for both materials. The higher scatter band with T_σ = 1:1.20 of the notched specimens was chosen in order for the generalised SN-curve to be conservative, since the results of the unnotched specimens showed a smaller scatter of T_σ = 1:1.15 for the 1.4016 steel and T_σ = 1:1.10 for the 1.7228 steel, due to the reduced scope of testing.

The following lines refer to the cyclic behaviour of the 1.4016 stainless steel. Above $N = 5 \cdot 10^5$ load cycles, it can be observed that late failures can occur for both specimen geometries. There are also mixed mode regions where both failures and run-outs occur. The slope k = 27.3 of the SN-curve of the unnotched specimens is quiet flat, which is well known for a stress ratio of R = 0 and a surface roughness $R_z \leq 3$ µm. The slope k = 6 of the SN-curve for notched specimens is in accordance with other results for notched specimens of steel.

The material behaviour of the 1.7228 steel is slightly different. Above $N = 1 \cdot 10^5$ load cycles, it can be observed that failures up to $N = 5 \cdot 10^5$ load cycles for unnotched specimens and $N = 8 \cdot 10^5$ load cycles for notched specimens can occur. There are also mixed mode regions, simillar to those already seen for the 1.4016 steel. The slope k = 38.2 of the SN-curve of the unnotched specimens is more flat than the slope of the unnotched 1.4016 specimens due to the higher strength and heat treatment. The slope k = 5.3 of the SN-curve for notched specimens is in accordance with other results for notched specimens of quenched and tempered steels.

Table 4 gives an overview of the characteristic values of all SN-curves in the nominal stress system, as mentioned above.

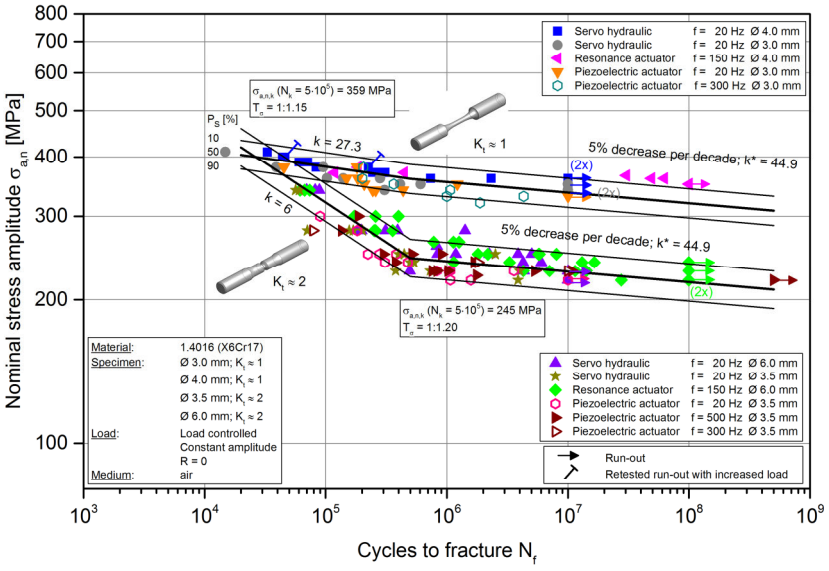

Fig. 5 - Test results of the 1.4016 steel with $K_t \approx 1$ and $K_t \approx 2$ tested at 20, 150, 300 and 500 Hz in air

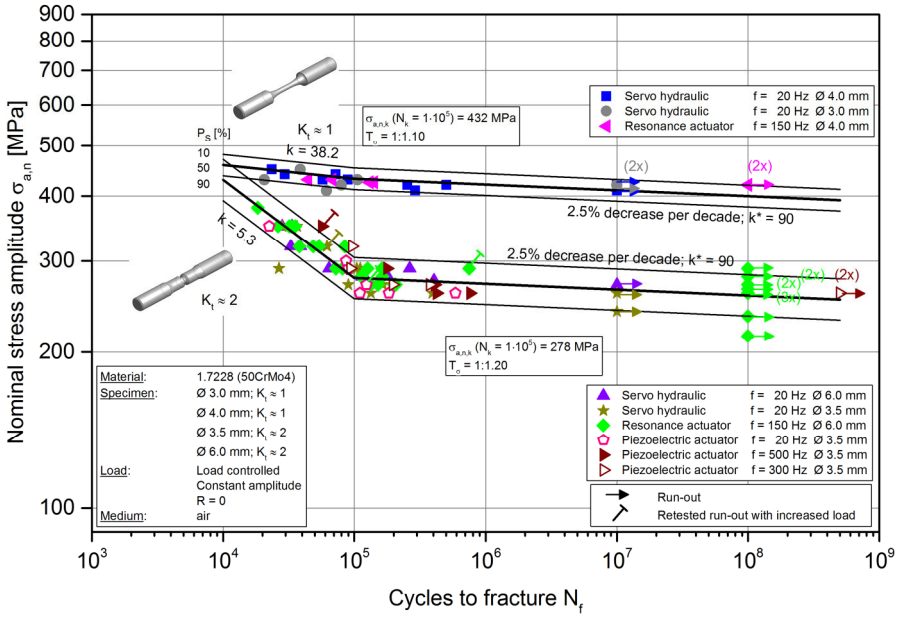

Fig. 6 - Test results of the 1.7228 steel with $K_t \approx 1$ and $K_t \approx 2$ tested at 20, 150, 300 and 500 Hz in air

Table 4 - Characteristic values of the SN-curves for both investigated materials in air

Material	K_t	k	k*	N_k	$\sigma_{a,n,k}$ [MPa]	T_σ	f [Hz]
1.4016	1	27.3	44.9	$5 \cdot 10^5$	359	1:1.15	20, 150, 300
	2	6.0	44.9	$5 \cdot 10^5$	245	1:1.20	20, 150, 300, 500
1.7228	1	38.2	90.0	$1 \cdot 10^5$	432	1:1.10	20, 150
	2	5.3	90.0	$1 \cdot 10^5$	278	1:1.20	20,150, 300, 500

Fatigue in E85 biofuel

In addition to the fatigue tests in air, fatigue tests in biofuel were performed. The SN- results of tests at 20, 150, 300 and 500 Hz load frequencies for the 1.4016 steel in E85 biofuel are shown for the unnotched specimens in Fig. 7 and for the notched specimens in Fig. 8. As outlined in the previous chapter, the nominal stress amplitude was plotted against the number of load cycles to fracture N_f in double logarithmic diagrams.

Referring to (Hickling, 2001), it can be clearly observed from both diagrams that, in the HCF regime, the fatigue strength decreased remarkably under simultaneous mechanical loading in contact with E85 biofuel. The decrease of the fatigue strength due to E85 biofuel at $N = 5 \cdot 10^6$ load cycles is approximately 26% at 20 Hz and 4% at 150 Hz test frequency for unnotched specimens. For the notched specimens, the decrease is approximately 57% at 20 Hz and 31% at 150 and 500 Hz, Fig. 9. In addition, no knee point N_K for the SN-curves of the unnotched and notched specimens is expected and the slope remains constant (Wendler-Kalsch, 2012; Hickling, 2001; Ebara, 2007).

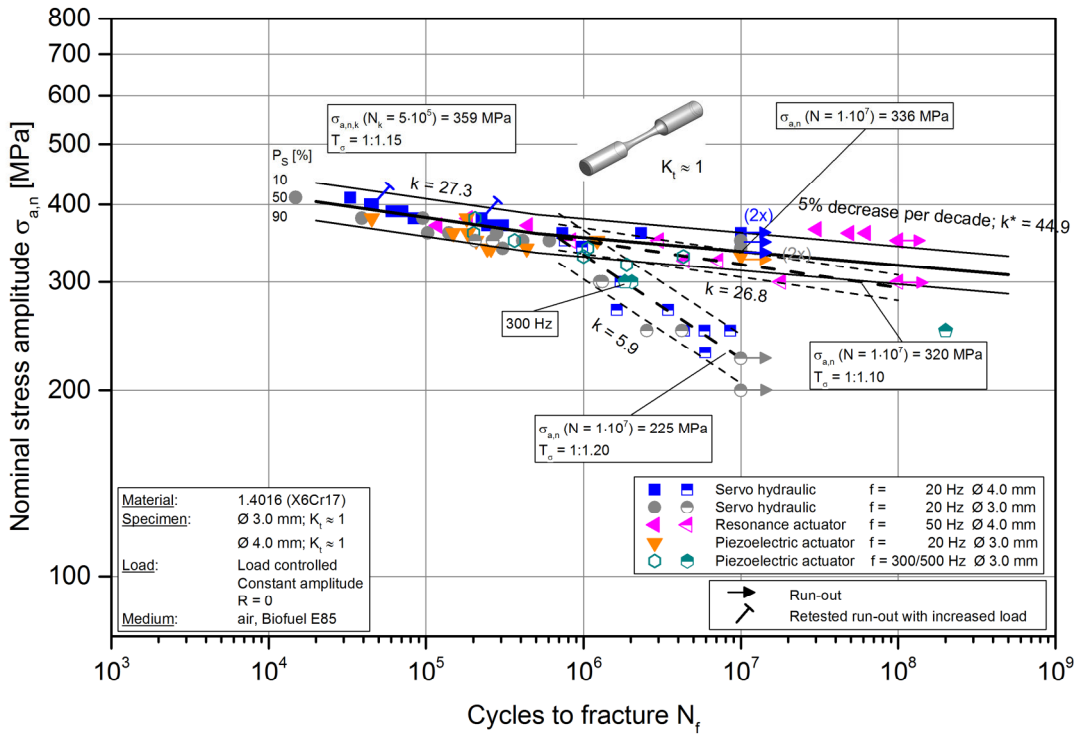

Fig. 7 - Test results of the 1.4016 steel with $K_t \approx 1$ tested at 20, 150, 300 and 500 Hz in E85 biofuel

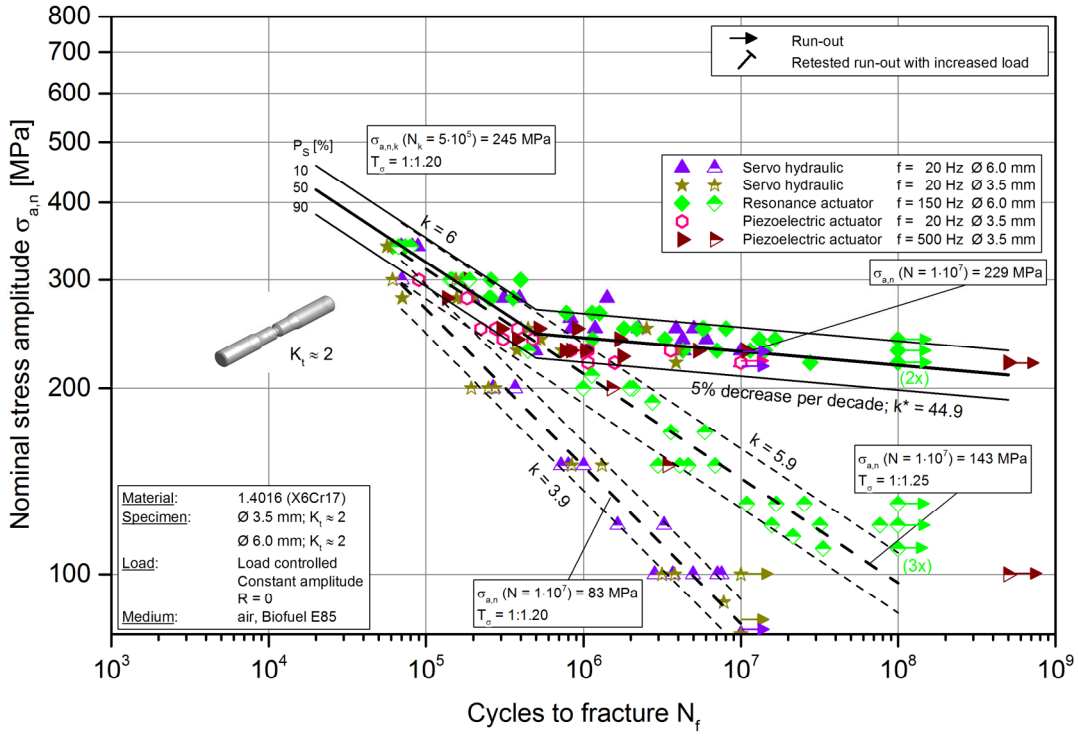

Fig. 8 - Test results of the 1.4016 steel with $K_t \approx 2$ tested at 20, 150, 300 and 500 Hz in E85 biofuel

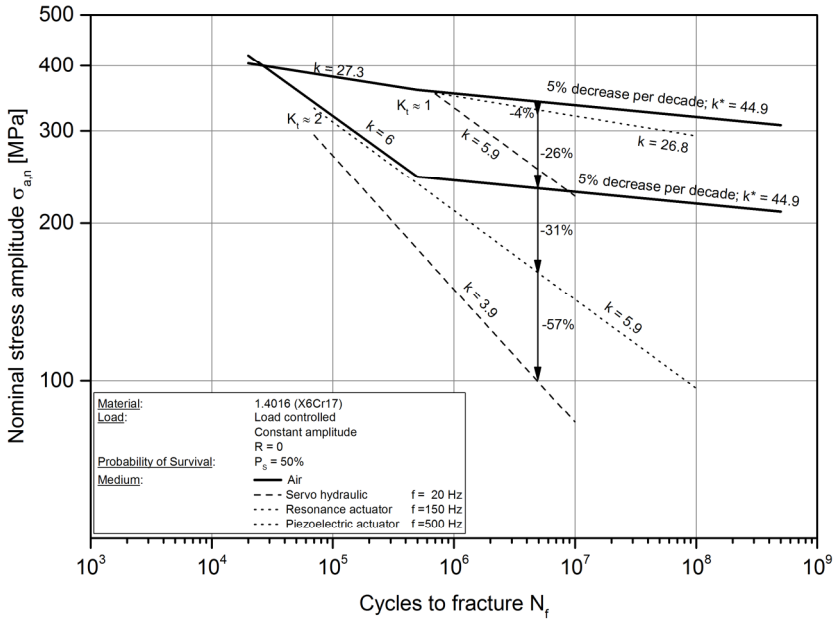

Fig. 9 - Decrease of the fatigue strength due to E85 biofuel. Fatigue strength decrease given at $N = 5 \cdot 10^6$ load cycles

Fig. 10 shows local corrosion spots at the surface of the specimen. As for the test results in air, multiple crack origins were found at the surface of all broken specimens, Fig. 11.

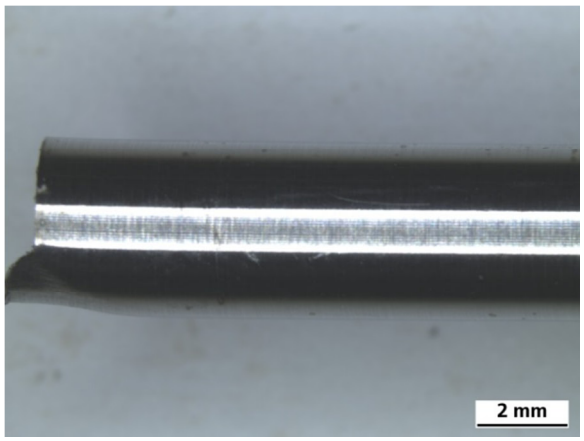

Fig. 10 - Slightly visible corrosive attack, e.g. localised corrosion spots on the surface occurred during the fatigue tests in contact with E85 biofuel with unnotched specimens

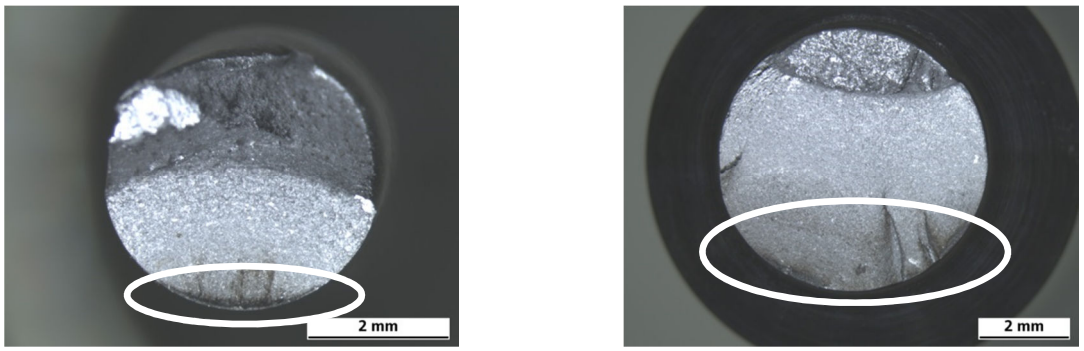

Fig. 11 - Fracture surface macro shot of unnotched (left) and notched (right) specimens - ellipses shows crack initiation area from surface

Closer observation of the fracture surface, by means of scanning electron microscopy (SEM), revealed intergranular crack formation at secondary crack sites merging to transgranular structures towards the core material, Fig. 12. This supports the assumption that intergranular corrosion (IGC) is the key initial factor for sample fracture. The susceptibility to IGC is dependent on the state of the material and its heat treatment, creating a shortage of chromium near the grain boundaries. In these areas, the chromium content locally drops below 13%, resulting in possible corrosion attack excavating partial and complete grains. By applying a cyclic mechanical load, persistent slip bands locally damage the passive layer and subsequently grain boundaries are being exposed to the corrosive medium. As a consequence, a crack is formed (Hickling, 2001).

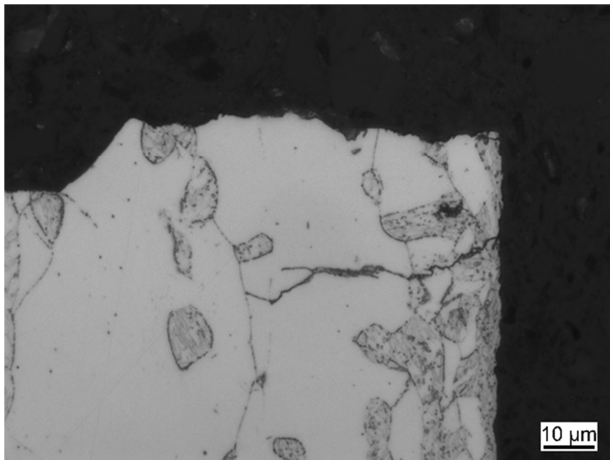

Fig. 12 - SEM image of secondary cracks with surface intergranular crack initiation for unnotched specimen

Fatigue in B20 biodiesel

The fatigue tests in B20 biodiesel give a totally different picture. A certain reduction of the fatigue strength cannot be observed even at a high number of load cycles ($N > 5 \cdot 10^6$), Fig. 13. The test results for $K_t \approx 2$ specimens are within the scatter band of the fatigue test results in air.

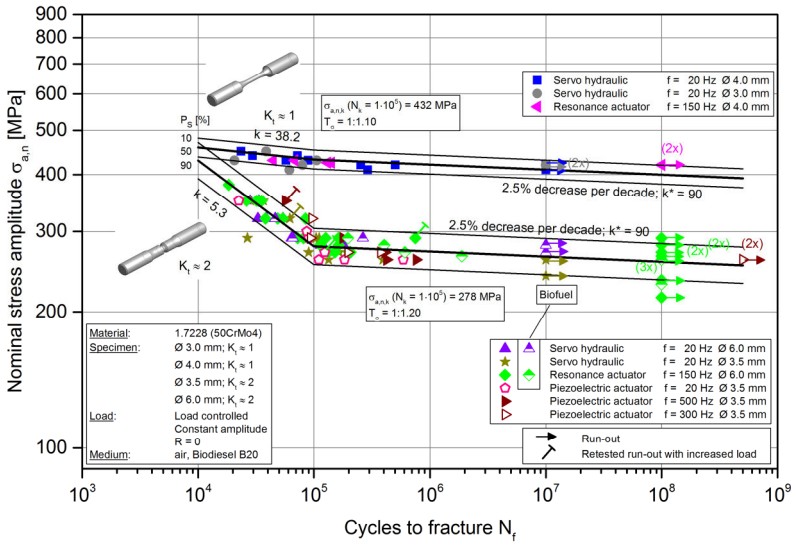

Fig. 13 - Test results of 1.7228 steel with $K_t \approx 1$ and $K_t \approx 2$ at 20, 150, 300 and 500 Hz in B20 biodiesel and air

As for the test results in air, crack origins were found at the surface of all broken specimens. SEM images of the fracture surface of samples tested in B20 biodiesel appear similar to the fractured surface tested in air, revealing transgranular crack formation, Fig. 14.

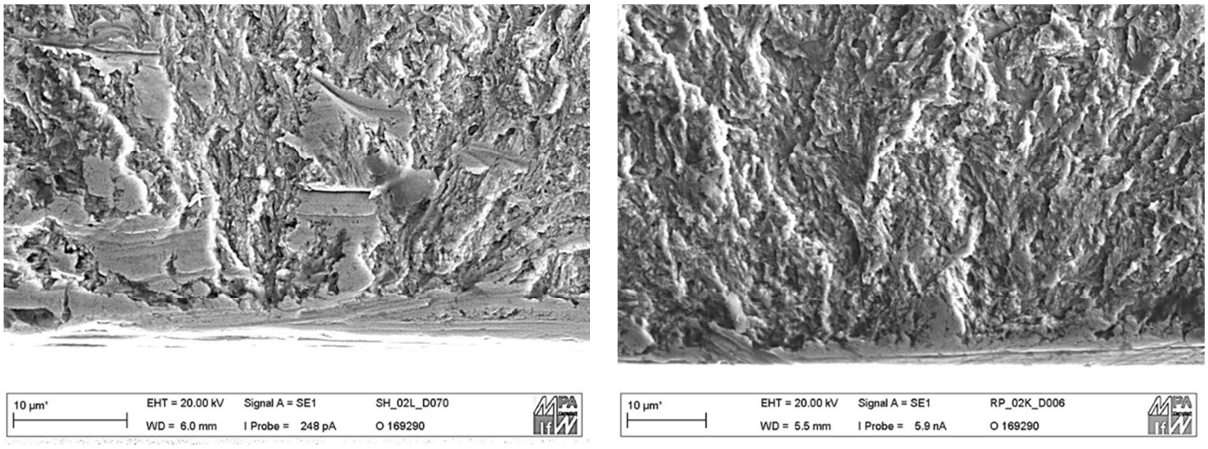

Fig. 14 - Comparison of SEM images of the fractured surface in air (left) and in B20 biodiesel (right)

DISCUSSION

In the following chapter, the cyclic behaviour of the stainless steel 1.4016 in contact with E85 biofuel will be discussed in detail.

The investigations on unotched ($K_t \approx 1$) and notched specimens ($K_t \approx 2$) exposed to E85 biofuel show that the fatigue life increases with increasing test frequency up to 150 Hz. Tests at 500 Hz test frequency show the same fatigue life as those at 150 Hz. The results are influenced by the corrosion fatigue of E85 biofuel and can therefore be related to testing technique and test frequency (temperature, strain rate, crack growth rate), notch sensitivity and time exposed to the medium.

Testing technique

All fatigue tests on the test rigs were conducted under load control. So, even during crack propagation, the nominal stress amplitude remains constant (Schneider, 2014). Therefore, an influence of the testing technique can be neglected.

Temperature

An influence caused by temperature on fatigue lifetime is not assumed, due to the fact that, in air, no warming of the specimens at higher stress amplitudes and no warming of the E85 biofuel during the tests was observed.

Strain rate

Tests using the piezoelectric actuator at 500 Hz result in significantly higher strain rates than those on the servo hydraulic test rig at 20 Hz, Fig.15. The strain rates at 150 Hz and at 500 Hz are 7.5 times and 25 times higher respectively, compared with the strain rates at 20 Hz.

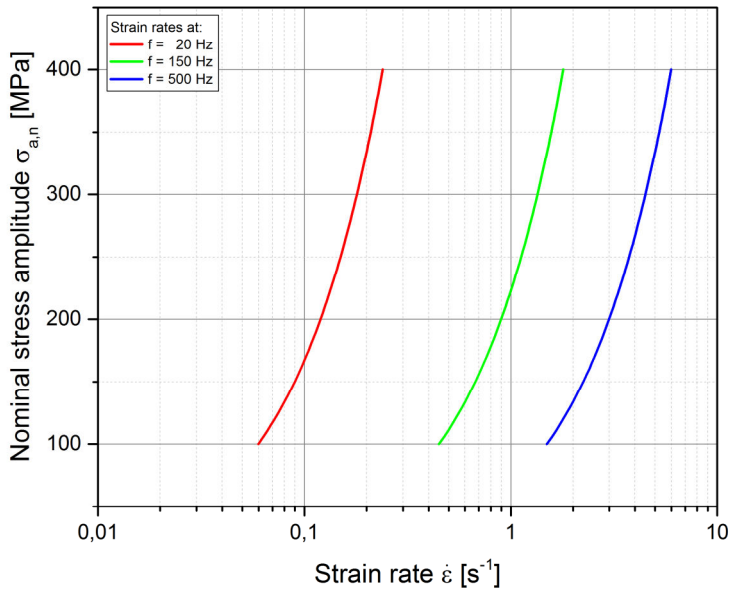

Fig. 15 - Comparison of strain rates at different test frequencies and a variety of nominal stress amplitudes

The strain rates shown in Fig. 15 can be calculated by equation (1)

$$\dot{\varepsilon} = 2\pi f \cdot \varepsilon_a \cdot \cos(2\pi f \cdot t) \quad (1)$$

It can be assumed that the influence on the lifetime of the strain rate can be identified separately for elastic and plastic strains (Schneider, 2014) by equation ().

$$\varepsilon = \varepsilon_{el} + \varepsilon_{pl} \quad (2)$$

Although there is a difference of 3.3 times in the strain rate between 150 Hz and 500 Hz, the number of cycles to failure is approximately the same. This supports the assumption that the increasing number of cycles with increasing frequency is not only driven by the increasing strain rate or, at least, only to a critical frequency. Further investigations and especially a strain-life-curve in air and biofuel and an elastic-plastic FE-simulation to determine the elastic and plastic strain influence are needed to clarify the influence by strain rate according to (Schneider, 2014).

Crack growth rate

The corrosion fatigue crack growth rates could also have an influence on the load cycles to fracture at different testing frequencies. The assumption that these rates are higher at low frequencies compared to high frequencies (less load cycles to failure at lower testing frequencies) is in agreement with previous studies (Adedipe, 2015; Knop, 2010; Dhinakaran, 2014). (Ishihara, 2006) also shows the influence of test frequency and load level on the type of corrosion crack growth and corrosion crack growth rate. The investigation of the influence of crack growth rates under corrosion impact was not part of this study, but should be taken into account in the future.

Notch sensitivity

In contrast to the fatigue results in air, the SN-results for local stress amplitudes of notched specimens show a lower fatigue strength at a higher number of load cycles to failure ($N_f > 1 \cdot 10^6$) than the unnotched specimens. Therefore, it is important to underline that the notch sensitivity in E85 is much higher than in air. Similar notch sensitivity behaviour was shown by (De la Cruz, 1998) for a steel in contact with sea water. However, it has to be considered that the well-known support effect of notched components ($\sigma_{a,loc.,notched} > \sigma_{a,loc.,unnotched}$) is lost with an increasing number of load cycles under corrosive impact in this 1.4016-85 Biofuel pairing.

Time exposed to E85 biofuel

The SN-results are plotted against the time t_f exposed to E85 biofuel until fracture. At different test frequencies, an influence of exposed time is observed for all fatigue tests. Results, excluding the tests on the notched specimens at a frequency of 500 Hz, are within a scatter band of $T_\sigma = 1{:}1.35$, which is typical for corrosion fatigue, Fig. 16. Investigations of (Schmid, 2013) have even shown a scatter band with $T_\sigma = 1{:}1.49$ for notched specimens in E85 biofuel. It was assumed that there is no additional knee-point.

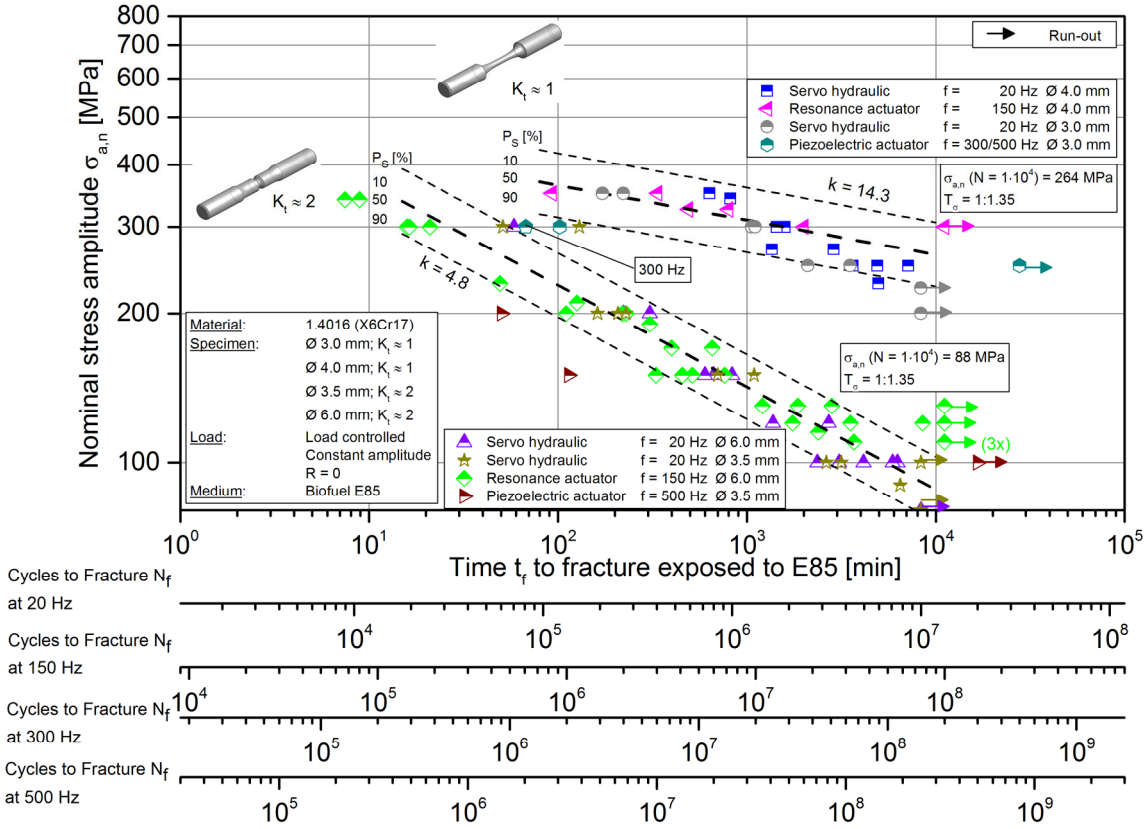

Fig. 16 - Results plotted against the time t_f exposed to E85 biofuel

The ratio of the local stress amplitude of notched specimens and unnotched specimens obtained at the same testing frequency is denoted by n and can be calculated according to equation ().

$$n = \frac{\sigma_{a,loc.}(K_t \approx 2)}{\sigma_{a,loc.}(K_t \approx 1)} = \frac{K_t \approx 2 \cdot \sigma_{a,n}(K_t \approx 2)}{\sigma_{a,n}(K_t \approx 1)} = \frac{K_t}{K_f} \qquad (3)$$

By calculation of the support factor n, it can be concluded that the different number of load cycles to fracture N_f at different testing frequencies is mainly influenced by the time t_f the specimens are exposed to corrosive media.

Fig. 17 shows the ratio n plotted against the time t_f to fracture exposed to E85 biofuel. The P_S = 50 % lines are close together and the lines at frequencies of 20 and 150 Hz are even lying on each other. By assuming a scatter band T_n = 1:1.35, which was mentioned before, there is an overlapping of the scatter bands.

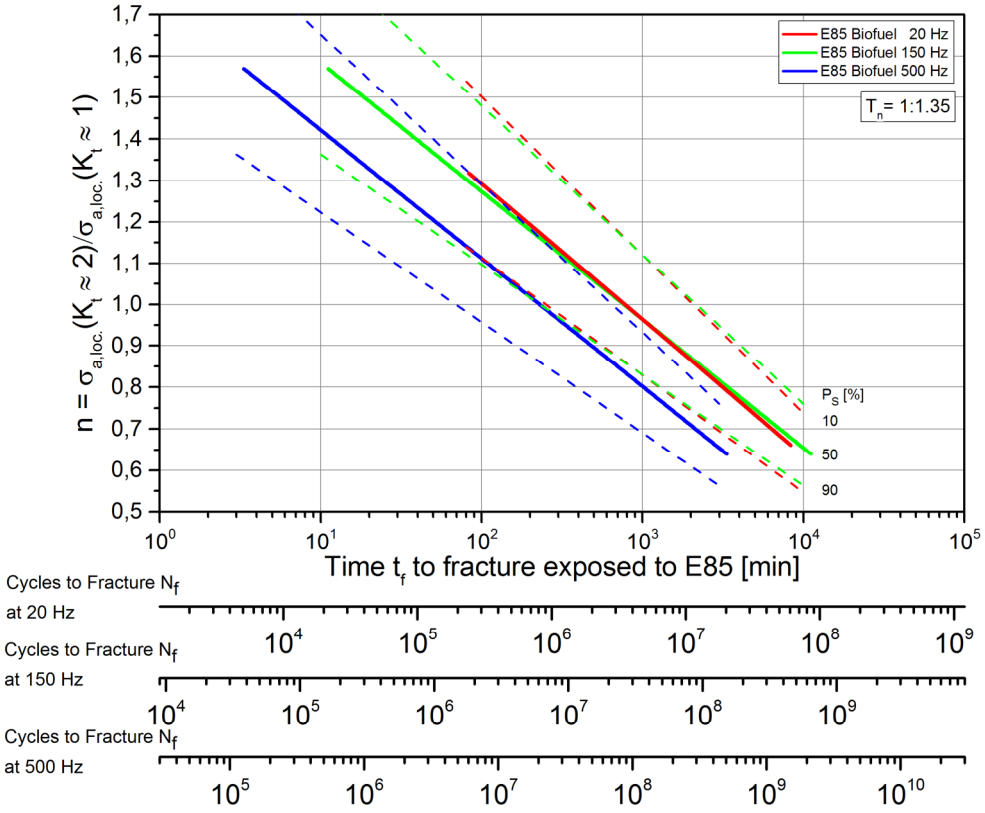

Fig. 17 - Support factor n plotted against the time t_f exposed to E85 biofuel

CONCLUSIONS

Load controlled SN-curves for stainless steel 1.4016 and quenched and tempered steel 1.7228 were determined in ambient air and biofuel on unnotched and notched specimens. This study has shown that there is a substantial decrease of the endurable stress amplitude dependent on the corrosive system consisting of biofuel and the type of steel.

The major observations are as follows:

- In air, E85 and B20 biofuel, all cracks initiated at the specimen surface.
- No frequency effect in air was observed.
- The decrease of the fatigue strength at $N = 5 \cdot 10^6$ load cycles due to E85 biofuel is approximately between 4-57% depending on the frequency and geometry of the specimens
- In E85 biofuel, the SN-results of notched specimens show less local fatigue strength for a higher number of load cycles than the unnotched specimen.
- In E85, the well-known support effect of notched components ($\sigma_{a,loc.,notched} > \sigma_{a,loc.,unnotched}$) is lost with an increasing number of load cycles under corrosive impact.
- A certain reduction of fatigue strength cannot even be observerd at a high number of load cycles of the quenched and tempered steel 1.7228 in B20 biodiesel
- SN-results in E85 biofuel show an increasing number of load cycles to fracture N_f with increasing test frequency f.
- Although long-term exposure tests in E85 biofuel were performed without mechanical load, showing no corrosion spots at all, the corrosive impact during fatigue tests reduces the fatigue strength significantly and this effect was supposed to be due to a superimposed intergranular corrosion mechanism.
- Long-term exposure tests in B20 biodiesel show no corrosion spots at all.

The major conclusions are as follows:

- Because of the plotting of ratio n against the time to fracture exposed to E85 biofuel, it has been determined that corrosion fatigue is mainly caused by the time influence.
- Additionally, a scatter band $T_\sigma = 1:1.35$, which is typical for corrosion fatigue, has been defined.
- Based on the obtained results, knowledge of non-corrosive behaviour of 1.7228 steel in contact with B20 biofuel has been obtained.

Further investigations suggested are:

- By considering only the load cycles until crack initiation, the influence of frequency, strain rate and time can be derived more precisely. This can be done by means of electrochemical measurements.
- A more detailed analysis of the crack initiation on the surface will be carried out through SEM investigations to obtain information regarding the crack initiation process and how it can be prevented or, at least, can be shifted to higher load cycles of fracture under corrosive impact.
- Clarification of the influence of frequency based on corrosion mechanism.

- Further tests should be performed in order to analyse other mechanical properties, such as strain-life curves, under corrosive impact.

ACKNOWLEDGMENTS

The author would like to acknowledge the Research Association for Combustion Engines (FVV) e.V. in co-operation with the German Research Funding Organisation (DFG) for its financial support within the research project "Ermüdung in korrosiven Kraftstoffen".

REFERENCES

[1]-O. Adedipe, F. Brennan, A. Kolios. Corrosion fatigue load frequency sensitivity analysis. Marine Structures, 2015, 42, pp. 115-136.

[2]-P. De la Cruz. Influence of sea water on the fatigue strength and notch sensitivity of a plasma nitrided B-Mn steel. Material Science Engineering: A, 1998, 247, pp. 204-213.

[3]-S. Dhinakaran, R.V. Prakash. Effect of low cyclic frequency on fatigue crack growth behavior of a Mn-Ni-Cr steel in air and 3.5% NaCl solution. Materials Science and Engineering: A, 2014, 609, pp. 204-208.

[4]-E. Haibach. Betriebsfestigkeit - Verfahren und Daten zur Bauteilberechnung, 3rd ed., Berlin, Heidelberg, Springer, 2006.

[5]-J. Hickling. Korrosionsschäden bei zusätzlicher mechanischer Beanspruchung. In: Systematische Beurteilung technischer Schadensfälle. 5th ed., Editor: G. Lange, Weinheim, New York, Chichester, Brisbane, Singapore, Toronto, WILEY-VCH, 2001.

[6]-M. Knop, J. Heath, Z. Sterjovski, S.P. Lynch. Effects of cycle frequency on corrosion-fatigue crack growth in cathodically protected high-strength steels. Procedia Engineering 2010, 2, pp. 1243-1252.

[7]-H. Neuber. Kerbspannungslehre, 2nd ed., Berlin, Göttingen, Heidelberg, Springer, 1958.

[8]-S. Ishihara, S. Daka, Z.Y. Nan, T. Goshima, S. Sunada. Prediction of corrosion fatigue lives of aluminium alloy on the basis of corrosion pit growth law. Fatigue & Fracture of Engineering Materials & Structures, 2006, Vol. 29, 6, pp. 472-480.

[9]-G. Rainer. Errechnen von Spannungen in Schweißverbindungen mit der Methode der Finiten Elemente. PhD-Thesis, TH Darmstadt, 1978.

[10]-S. Schmidt. Untersuchung zum Ermüdungsverhalten von mittel- und hochfesten Stählen bei sehr hohen Lastspielzahlen unter Berücksichtigung von Schwingungsrisskorrosion infolge moderner Biokraftstoffe. PhD-Thesis, Bremen University, 2013.

[11]-N. Schneider. Influence of Frequency and Testing Technique on the Fatigue Behaviour of Quenched and Tempered Steel in the VHCF-Regime. Advanced Materials, 2014, 891, pp. 1430-1435.

[12]-C.M. Sonsino. Course of SN-curves especially in the high-cycle fatigue regime with regard to component design and safety. International Journal of Fatigue, 2007, 29, pp. 2246-2258.

[13]-E. Wendler-Kalsch. Schwingungsrisskorrosion (SwRK), Korrosionsermüdung. In: Korrosionsschadenkunde. 1st ed. 1998, reprinted 2012, Berlin, Heidelberg, Springer-Verlag, 2012.